A&A 501, 965–971 (2009)
DOI: 10.1051/0004-6361/200811194

Astronomy & Astrophysics

Search for associations containing young stars (SACY)

II. Chemical abundances of stars in 11 young associations in the solar neighborhood⋆,⋆⋆

P. Viana Almeida[1,2,6], N. C. Santos[1,6], C. Melo[3], M. Ammler-von Eiff, C. A. O. Torres, G. R. Quast, J. F. Gameiro, and M. Sterzik[2]

[1] Centro de Astrofísica, Universidade do Porto, Rua das Estrelas, 4150-762 Porto, Portugal
[2] ESO, Alonso de Cordova 3107, Casilla 19001, Vitacura, Santiago, Chile
e-mail: palmeida@eso.org
[3] ESO, Karl-Schwarzschild-Str.2, 85748 Garching bei München, Germany
[4] Centro de Astronomia e Astrofísica da Universidade de Lisboa, Observatório Astronómico de Lisboa, Tapada da Ajuda, 1349-018 Lisboa, Portugal
[5] Laboratório Nacional de Astrofísica/ MCT, Rua Estados Unidos 154, 37504-364 Itajubá (MG), Brazil
[6] Departamento de Matemática Aplicada, Faculdade de Ciências da Universidade do Porto, Portugal

Received 20 October 2008 / Accepted 26 March 2009

ABSTRACT

The recently discovered coeval, moving groups of young stellar objects in the solar neighborhood represent invaluable laboratories for studying recent star formation and searching for high metallicity stars that can be included in future exo-planet surveys. In this study, we derived through an uniform and homogeneous method stellar atmospheric parameters and abundances for iron, silicium, and nickel in 63 post-T Tauri stars from 11 nearby young associations. We further compare the results with two different pre-main sequence (PMS) and main sequence (MS) star populations. The stellar atmospheric parameters and the abundances presented here were derived using the equivalent width of individual lines in the stellar spectra by assuming the excitation/ionization equilibrium of iron. Moreover, we compared the observed Balmer lines with synthetic profiles calculated for model atmospheres with a different line-formation code. We found that the synthetic profiles agree reasonably well with the observed profiles, although the Balmer lines of many stars are substantially filled-in, probably by chromospheric emission. Solar metallicity is found to be a common trend in all the nearby young associations studied. The low abundance dispersion within each association strengthens the idea that the origin of these nearby young associations is related to the nearby star-forming regions (SFR). Abundances of elements other than iron are consistent with previous results for Main Sequence stars in the solar neighborhood. The chemical characterization of the members of the newly found nearby young associations, performed in this study and intended to proceed in subsequent works, is essential to understanding and testing the context of local star formation and the evolutionary history of the galaxy.

Key words. stars: pre-main sequence – stars: abundances – open clusters and associations: general – stars: fundamental parameters – solar neighborhood

1. Introduction

For many years the canonical star-forming regions (such as Taurus, Rho-Oph, Sco-Cen complex) were the closest places for studying astrophysical issues related to the (local and recent) star-formation process.

The confirmation by Kastner et al. (1997) of an early proposal by Gregorio-Hetem (1992) that a small group of young stars around TW Hydra would form a loose association sharing common characteristics, such as age, distance, X-ray emission level, and radial velocities, showed that young stars can be found at a much closer distance than previously thought.

Since then, a dozen of young nearby associations have been identified (see reviews by Zuckermann & Song 2004; Torres et al. 2003, 2008). These associations are valuable laboratories for addressing recent star formation in the solar neighborhood. Because of their proximity, they may yield important information to help our understanding of a wide variety of open issues about the formation and evolution of planetary systems.

Because typical ages of these groups match the timescales for disk dispersal (e.g., Spangler et al. 2001) and planet formation (Pollack et al. 1996), they also constitute interesting targets for exoplanet searches.

As previous studies strongly suggest (e.g., Gonzalez 1997; Gonzalez et al. 2001; Santos et al. 2001, 2004, 2005; Fisher & Valenti 2005), planet-host stars may display a higher metal content. Consequently, it becomes relevant to search for a high metallicity sample among young stars, such as these post-T Tauri stars (PTTS), to focus more effectively on future planetary search projects.

In this context, it is important to carry out a chemical characterization of the newly-found loose associations and compare them with the typical stellar population, both the older MS (Sousa et al. 2008) and the younger PMS

⋆ Based on observations collected with the UVES spectrograph at the VLT/UT2 8.2-m Kueyen Telescope (ESO run ID. 079.C-0556(A)) at the Paranal Observatory, Chile.
⋆⋆ Tables 1, 2 and 5 are only available in electronic form at http://www.aanda.org

(James et al. 2006; Santos et al. 2008) found near the Sun. This comparison could provide a clearer understanding of the origin of the stellar population in the solar neighborhood.

In this study, we present stellar parameters and chemical abundances for 63 PTTS in 11 young nearby associations, specifically AB Doradus (AB Dor) (Zuckermann et al. 2004; Torres et al. 2008), Argus (Torres et al. 2008), β Pictoris (Zuckermann et al. 2001; Song et al. 2003; Torres et al. 2006, 2008), Carina, Columba (Torres et al. 2008), ε Chamaeleon (Barrado y Navascués 1998; Mamajek et al. 2000; Torres et al. 2008), R Coronae Australis association (R CrA) (Neuhäuser et al. 2000), Lower Centaurus-Crux (LCC), Octans (Torres et al. 2008), Tucana-Horologium (Tuc-Hor) (Zuckermann & Webb 2000; Torres et al. 2000, 2008), and Upper Scorpius (US). Furthermore, we compare our results with those for a sample of PMS and MS populations in the solar neighborhood taken from the literature. A subsequent discussion of the implications of the study is presented.

2. Sample and observations

The 63 objects used in this study are listed in Table 1. They were selected from Torres et al. (2006) based on the following criteria: i) they have been classified as a highly probable or probable member of a given association according to Torres et al. (2008); ii) they have $v \sin i$ lower than 15 km s^{-1} to avoid strong line-blending; iii) to the best of our knowledge, they are all single stars; and iv) they are young (younger or of Pleiades age) based on the equivalent width of their Li I 6708 line.

High-resolution ($R = \frac{\lambda}{\Delta\lambda} = 50\,000$ in both arms) spectroscopic observations carried out between March and September 2007 were performed using the DIC#1 390+580 mode with the UVES spectrograph (Dekker et al. 2000) at the VLT/UT2 8.2-m Kueyen Telescope (Paranal Observatory, ESO, Chile). The spectra obtained cover a wavelength interval from 4800 to 7000 Å with a gap between ~5755 and 5833 Å.

Data reduction was performed with the UVES pipeline by carrying out the usual steps for echelle data reduction. For most of the targets, multiple exposures had to be taken to avoid saturation. Once extracted, the multiple spectra for a given target were shifted to rest velocity and combined to produce a high SNR (~150–200) final spectra.

The synthesis of the Hα and the Hβ profiles was carried out using the 2D extracted spectra (i.e., the intermediate pipeline product prior to the merging of the spectral orders). This step is necessary to normalize properly the regions of the Balmer profiles to the relative continuum. We refer the reader to the work of Ammler-von Eiff & Santos (2008) for a detailed explanation of the different steps of the reduction procedure.

The comparison data for MS dwarfs used in this paper were taken from Sousa et al. (2008, hereafter SOU08) and Gilli et al. (2006, hereafter GI06), whereas the WTTS comparison sample comes from Santos et al. (2008, hereafter SA08).

3. Analysis of spectra

3.1. Stellar parameters and abundances

The stellar parameters and iron abundances shown here were determined using the same methodology described in Santos el al. (2004). Preliminary work consisted in measuring the equivalent widths (EW) of a set of FeI and FeII lines on the collected spectra using the IRAF splot tool and a Gaussian fitting procedure. The line-list of the FeI/FeII species considered was taken from the aforementioned paper and consists essentially of weak lines with an extended range of excitation potentials to ensure a robust fitting.

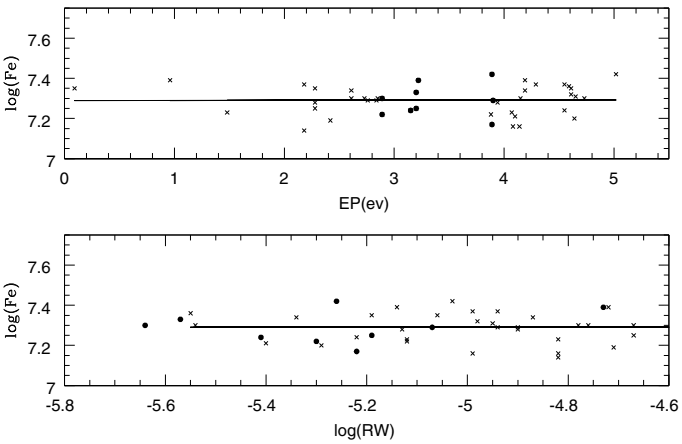

Fig. 1. Individual line FeI (crosses) and FeII (filled circles) abundances as a function of the excitation potential (*top panel*) and the reduced equivalent width, RW = EW/λ (*bottom panel*) for one of the coolest stars in the sample, CD-22 11502 in the US association. In both cases, no systematic dependence of the derived abundances is seen as a function of these two quantities.

A spectroscopic analysis was then performed with a recent version (2002) of the radiative transfer code MOOG (Sneden et al. 1973) using the local thermodynamic equilibrium (LTE), constant flux, blanketed atmospheric models, taken from the ATLAS9 stellar grid of Kurucz (1993).

The four fundamental parameters, effective temperature ($T_{\rm eff}$), surface gravity ($\log g$), microturbulence ($\xi_{\rm t}$) and the iron abundance ([Fe/H]) presented here were furthermore derived by imposing the Fe excitation/ionization equilibrium.

In Fig. 1, we show an example of the two final fits (slope ~0.00) obtained for a cool star (CD-22 11502) with a $T_{\rm eff}$ of 4951 K. Of particular interest in those plots is the small dispersion in the iron abundances found.

The errors affecting the parameters were computed with the very same method as in Gonzalez (1998). Final derived parameters, abundances, and uncertainties are presented in Table 2. We should point out that the errors displayed in this study only represent relative uncertainties. They do not represent absolute uncertainties in the atmospheric parameters but rather underlying errors related to the method used in this study.

In addition to iron, abundances for Si and Ni were also derived. We refer the reader to Santos et al. (2006) and GI06 for a description of the procedures and atomic line-list used. Resulting abundances and errors for these elements are given in Table 5. Furthermore, abundance ratios [X/Fe] (with X = Ni and Si) were compared with those from GI06, who applied the same method, line list, and atmospheric models.

All abundances displayed here are differential with respect to the Sun. The following solar parameters were adopted: $T_{\rm eff}$ = 5777 K, $\log g$ = 4.44 dex, $\xi_{\rm t}$ = 1.00 km s^{-1}, $\log \varepsilon_{\rm Fe}$ = 7.47 dex. Solar abundances for these for Si and Ni were taken from Anders & Grevesse (1989).

In a similar way to previous studies of PMS stars (Padgett 1996; James et al. 2006; Santos et al. 2008), the microturbulence values obtained for the PTTS studied here are higher than the typical ones usually exhibited by MS field dwarfs. The reason for these larger values is unknown. It has been suggested that this may be caused by enhanced magnetic field activity, which is

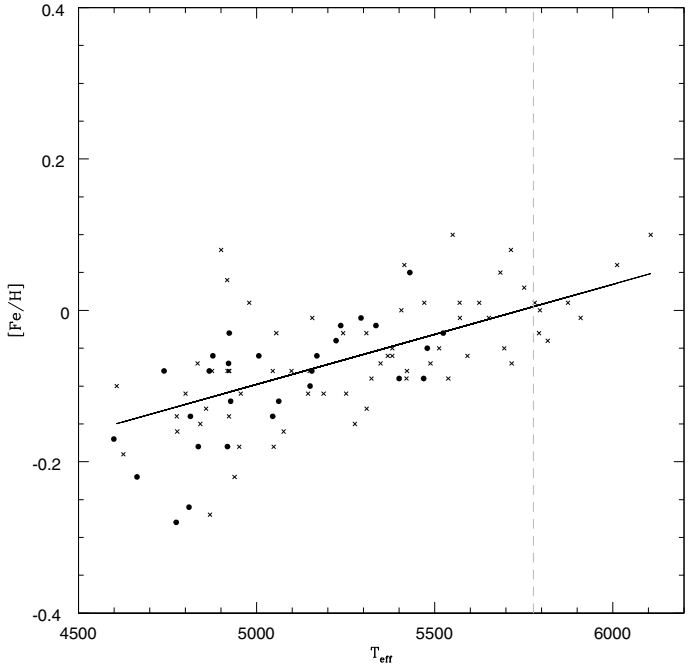

Fig. 2. $T_{\rm eff}$ vs. [Fe/H] plot for the stars studied in this work (crosses) and that of SA08 (filled circles). The solid black line represents a simple least square fit of the initial values found. The slope of the line is of about 0.13 dex per 1000 K. The dashed vertical line represents the solar value used as a reference.

known to be considerably stronger during the pre-main sequence phase (SA08).

We plotted the microturbulence against the various parameters involved in the determination, such as $T_{\rm eff}$, log g, [Fe/H], and $\upsilon \sin i$ to detect possible trends that could represent the origin of these higher microturbulence values. Despite a smooth dependence on temperature, the cooler the star, the higher the value of $\xi_{\rm t}$, it seems that there is no apparent influence of other factors such as the $\upsilon \sin i$ of the stars. In this context, we were unable to understand whether these results come from the intrinsic physics of the stars studied here or, for instance, from the atmospheric models used.

3.2. [Fe/H] correction

After inspecting the atmospheric parameters and Fe abundances shown in Table 2, we note that in the temperature range from 4500 K to 5500 K the determined values of [Fe/H] experience an overall increase as a function of $T_{\rm eff}$ (Fig. 2). This is true for any given association studied. Overplotting the [Fe/H] and $T_{\rm eff}$ derived by SA08 on our own values, we can clearly see that the trend reported by these authors is similar to the one found in our analysis.

The trend shown in Fig. 2 contradicts the standard idea that stars originated within the same cloud will show a similar abundance pattern. Therefore, we believe that the slope seen in Fig. 2 is likely to be caused by systematic errors. It is known that PMS stars often display enhanced stellar activity, and spectroscopic results, such as atmospheric parameters, may become modulated by stellar spots, strong magnetic fields, or NLTE effects. Moreover, as the star becomes cooler, the line blending becomes stronger, causing a possible [Fe/H] underestimation. An extensive study of the influence of stellar spots on deriving stellar parameters can be found, for instance, in Morel et al. (2004).

Table 3. Average Fe abundances and standard deviations.

Association	⟨[Fe/H]⟩	σ	⟨[Fe/H]⟩*	σ*	$N_{\rm stars}$
AB Dor	–0.01	0.09	0.04	0.05	12
Argus	–0.03	0.05	0.02	0.06	7
β Pic	–0.13	0.08	–0.01	0.08	1
Carina	–0.07	0.04	0.01	0.04	7
Columba	–0.05	0.07	–0.03	0.07	6
R CrA	–0.08	0.00	0.00	0.00	2
ϵ Cha	0.01	0.05	0.03	0.05	1
LCC	–0.06	0.05	0.02	0.05	7
Octans	–0.09	0.06	–0.03	0.05	1
Tuc-Hor	–0.06	0.09	–0.03	0.05	9
US	–0.11	0.10	–0.02	0.09	10
Total sample	–0.06	0.08	0.00	0.06	63
SA08	–0.08	0.09	0.04	0.06	28
SOU08	–0.10	0.24	–	–	450

A possible influence of the atmospheric models used, optimal in the temperature window considered, cannot be discarded. However, tests carried out in Sect. 3.3 (see below) do not support this hypothesis. A robust comparison sample with different stellar models is needed to understand whether the trend observed is a by-product of the analysis employed or if it has a true origin in the stars studied.

Regardless of the origin of this effect, a first-order correction was carried out by performing a simple linear least squares fit to the data points in Fig. 2. We then subtracted the fitted relation from all [Fe/H] values, assuming that at the solar temperature no correction was required. The same correction was applied to the SA08 metallicities. The [Fe/H] values corrected by this method are shown in the asterisked columns in Tables 2 and 3.

By looking at the corrected results in both of these two tables, we see that a slightly smaller dispersion within each association is found. However, since we are unable to ascertain a physical justification for the correction applied above, only the original (uncorrected) values of [Fe/H] obtained were considered throughout the paper.

3.3. Hα and Hβ synthetic profiles

To establish in greater detail the consistency of the stellar parameters, and more specifically of $T_{\rm eff}$ determined using the method described in Sect. 3.1, we computed the synthetic profiles for the two Balmer lines, Hα and Hβ. It has been shown that H-line profiles are very sensitive to temperature variations, but quite insensitive to gravity and metallicity variations (see e.g., Fuhrmann et al. 2004, and references therein). This is why it is possible to derive quite accurate stellar $T_{\rm eff}$ from the hydrogen lines.

Ten stars of the entire sample were used, half of them featured in our analysis as having $T_{\rm eff}$ lower than the Sun and the other half with approximately solar $T_{\rm eff}$.

The profiles were calculated with the LINFOR line-formation code using the MAFAGS model atmospheres as described in Fuhrmann et al. (2004, and previous papers), Ammler (2006), Ammler-von Eiff & Santos (2008). We then compared the synthetic profiles with those observed in the stellar spectra. The method used consisted of selecting the $T_{\rm eff}$, log$g$, $\xi_{\rm t}$ and [Fe/H] from Table 2 to derive two profiles for both the Hα and Hβ lines of each star in the sample. One profile is calculated for the lower limits to all parameters and one for the upper limits to all parameters given by the uncertainty range in the parameters

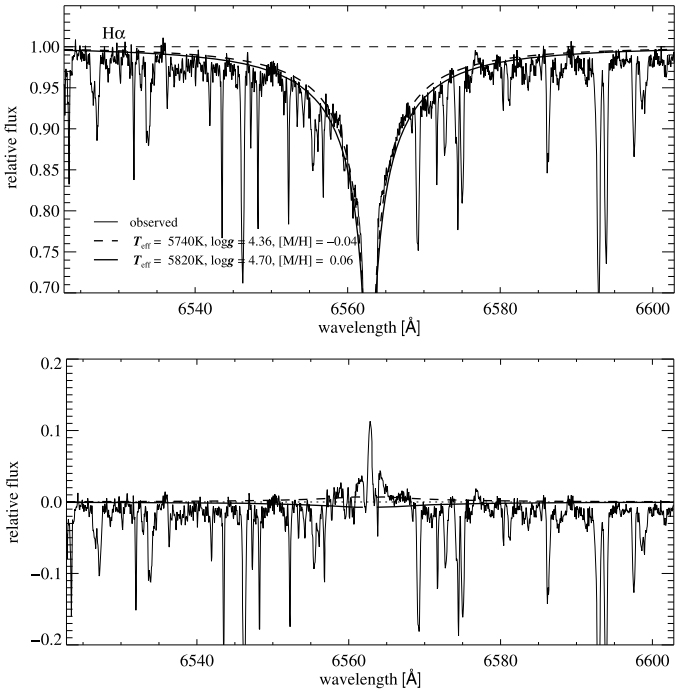

Fig. 3. Observed and synthetic Hα profile for the star HD47875. The horizontal dashed line represents the assumed continuum. One profile was computed to a lower limit (dashed line) on all parameters and another to an upper limit (solid line). The residuals of the yielded comparison are displayed in the lower panel.

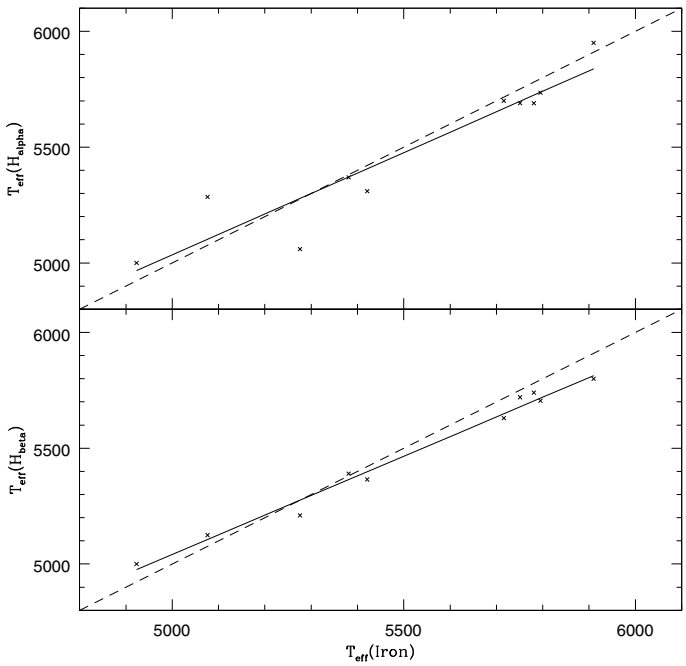

Fig. 4. Comparison between effective temperatures derived using iron lines with those obtained through synthesis of the line profiles of Hα and Hβ. Both solid lines represent linear least square fits performed to the data (with a slope of ~0.9). For clarity we also show the ideal 1:1 relation (dashed line).

in Table 2. This is a good choice since reducing log g and [Fe/H] has the same effect on the profiles as reducing $T_{\rm eff}$, which maximizes the effect of the uncertainties onto the synthetic profiles.

We note that the comparison between the synthetic and the observed profiles is only valid down to relative flux levels of about 70 percent. Below this value, deviations due to NLTE start to play a role (Fuhrmann et al. 2004, and previous papers).

For some stars, the Hα lines seemed strongly affected by chromospheric emission, the strongest displayed by CD-361785. The Hβ line seems less affected throughout the whole sample. We decided to probe the influence of this emission on the Balmer line wings and to determine implications for derivation of effective temperature by computing the residuals displayed in the lower panel of Fig. 3.

In this plot, the limiting synthetic profiles were not subtracted from the observed profile. Instead, an additional synthetic profile was calculated based on the nominal stellar parameters (regardless of the error bars). This synthetic profile then was subtracted from the limiting synthetic profiles as well as from the observed profile. These differences are shown in the lower panel of Fig. 3.

By studying these residuals, it turned out that for the chromospherically active stars, Hβ appeared to be a more suitable choice for confirming effective temperature. However, there are usually many lines in the Hβ region and the wings cannot be properly traced. Still, Hβ can be used to confirm $T_{\rm eff}$ when Hα becomes useless, e.g., in the example of CD-361785.

In the two panels of Fig. 4, we plot the effective temperatures obtained through the iron excitation/ionization equilibrium against those derived by the synthesis of the Hα and Hβ line profiles. No clear (and strong) systematic difference is seen between the $T_{\rm eff}$ derived by the two methods in the temperature range covered by the stars studied in this paper. It is, therefore, wise to claim that the relation seen in Fig. 4 can be extended to all 63 stars considered in this study.

As a conclusion, we may assume that the temperatures derived from the analysis of the FeI and FeII lines agree reasonably well with those obtained by fitting the H-line profiles (with the exception of the star CD-361785) even though for the latter method another set of model atmospheres and another line-formation code were used. A small systematic temperature difference may be present in the data, although not higher than ~100 K from peek to peek. This difference could account for no more than ~0.06 dex in the derived iron abundances (propagating the error in the temperature), and cannot thus fully explain (by a factor of 2) the [Fe/H] trend observed in Fig. 2.

We should note, however, that we are considering the effective temperatures derived using H-line profiles as a reference. These values are also unlikely to be free from systematic errors, which could arise from e.g. greater difficulties of placing the continuum for the lower temperature stars, or from the filling-in of the profile for the very active stars.

3.4. Astrometric gravities

In addition to the test performed for effective temperature, we checked whether there was any particular difference between our stellar gravities and those obtained by applying Eq. (1) in Santos et al. (2004), using Hipparcos parallaxes (ESA 1997), hence accurate luminosities and $T_{\rm eff}$, which enable mass estimation using evolutionary tracks.

We first note that any conclusion inferred from this comparison should be interpreted with caution. The variability of the PTTS analysed, the uncertainties attached to the PMS evolutionary tracks used for mass estimation are amongst some of the reasons why we must be careful in addressing stellar parameters coming from evolutionary stellar models. Indeed, stars in

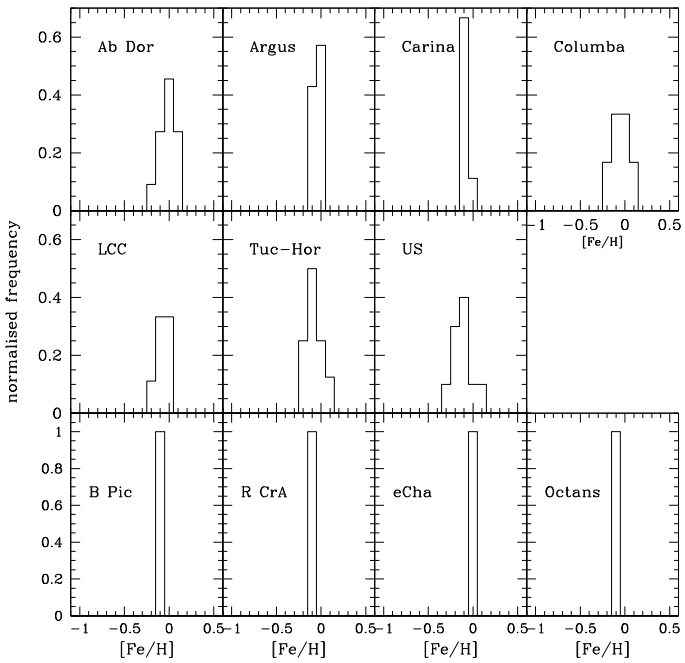

Fig. 5. Weighted distribution of our PTTS sample as a function of [Fe/H] for each association studied.

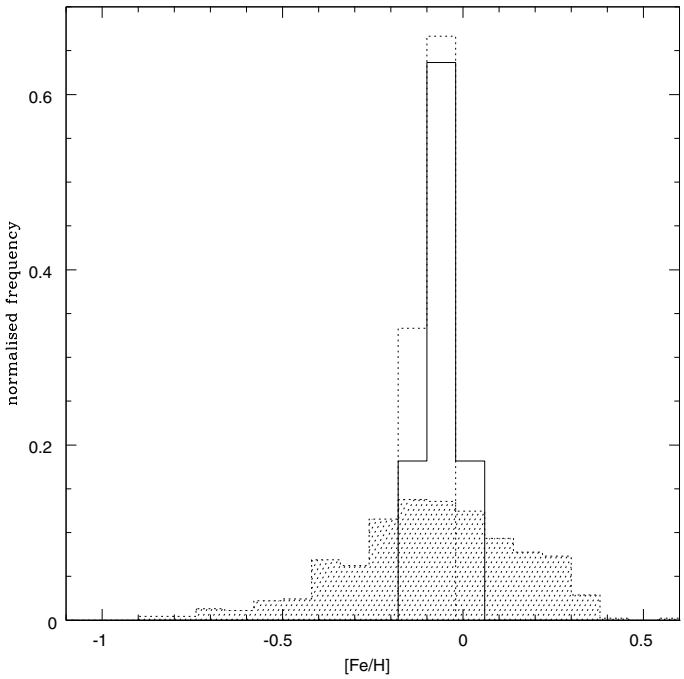

Fig. 6. Metallicity-weighted distribution of the 6 SFR (dotted line) studied by SA08, of our 11 associations (solid line) and of the 450 MS stars (shadowed area) in the solar neighborhood plotted as functions of [Fe/H].

this phase of evolution are experiencing considerable structure contraction, which can drive radius, age, and mass estimations completely off course. At the same time, Hipparcos parallaxes are not always sufficient for performing a complete sample comparison (in some cases the uncertainties are quite high).

Notwithstanding these considerations, we searched for parallax (π) information in the Hipparcos catalogue to compute stellar astrometric masses that could be used in the gravity comparison. Unfortunately, from the 63 stars of Table 2 only 19 were featured in the catalogue. A complete sample comparison between the gravities inferred from the two different techniques was therefore not feasible.

Regardless of this, we estimated the mass for these 19 stars by using the isochrones of Shaller et al. (1992) and Shaerer et al. (1992, 1993) by interpolating the V absolute magnitudes in Table 1 and the $T_{\rm eff}$ of Table 2 in the resulting Hertzprung-Russel diagram. For the bolometric correction, we used the calibration by Flower (1996).

A comparison between the two sets of surface gravities showed that the parallax-based values are, on average, higher than those derived by the use of FeI and FeII lines. The average offset is about ~0.46 dex, with an rms of 0.32 dex. The values derived using Hipparcos gravities for the 19 stars (with an average of 4.80 dex) are clearly higher than expectation, while those derived by the method described in Sect. 3.1 (average of 4.33 dex) are usually within the expected range of values.

4. Results

4.1. Fe abundance and atmospheric parameters

By analysing the metallicity values of the different stars and the relatively small dispersions obtained (Table 2), we see that the trend described in Sect. 3.2 rather than limiting the conclusions, strengthens the notion that the metallicities of all associations studied here have approximately the same value, namely, around solar (Fig. 5). The typical standard deviations are within the uncertainty range of the [Fe/H] determinations.

Table 4. Weighted average of the Fe abundance and standard deviation before and after correction (asterisked columns).

Sample	⟨[Fe/H]⟩	σ	⟨[Fe/H]⟩*	σ*	$N_{\rm SFR}$
Total	–0.06	0.04	0.00	0.03	11
SA08	–0.08	0.03	0.06	0.03	6

In Fig. 6 the normalized distributions of the average values of [Fe/H] for the 11 associations of our sample, and for two comparison samples from SA08 and SOU08 are shown. As we can seen in this figure and also in Table 4, low dispersion values (at the level of individual errors) are also found if the dispersion in the average metallicity of all 11 associations studied in this paper and the SFRs analysed by SA08 are considered.

A striking feature of Fig. 6 is that while the MS population show a broad distribution of metallicities spanning over more than 1.0 dex, the PMS sample of SA08 and the nearby young associations overlap almost entirely. Both distributions could be combined without increasing the dispersion in the final [Fe/H] distribution.

In summary, *the nearby young associations and the SFRs share the same metallicity. Within the errors, both show solar metallicities with very little (below 0.1 dex) dispersion around the mean [Fe/H] value*. Although the precise formation mechanism of these young associations is unknown, our result is further evidence suggesting that they are all related to the nearby SFRs (Torres et al. 2008). Our results bring further support to the idea suggested by SA08 that super metal-rich stars (with metallicity clearly above solar) found in the solar vicinity may have been formed in inner Galactic disk regions.

4.2. Other elements

Several abundance surveys across the Galaxy over the years have shown that structural components of the Milky-Way (bulge,

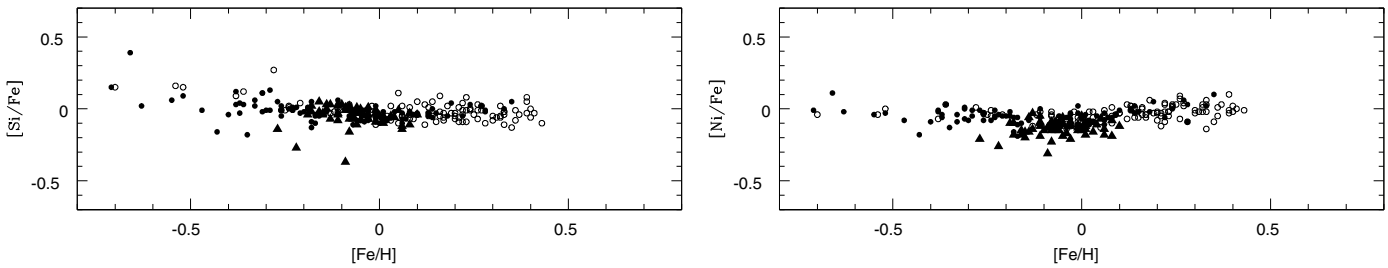

Fig. 7. [X/Fe] vs. [Fe/H] for the PTTS in the sample (filled triangles) and for two comparison sets of stars with (open circles) and without planetary-mass companions (filled circles) in the solar neighborhood from the literature.

Table 6. Average [X/H] abundance, corresponding standard deviation, and average number of lines used for abundances determination.

Species	⟨[X/H]⟩	σ	⟨N⟩
Si	–0.11	0.1	8.4
Ni	0.01	0.10	23.3

thin, and thick disk and halo) exhibit characteristic abundance patterns for α-elements and iron-peak elements with respect to iron and oxygen (see e.g., McWilliam 1997; Nissen et al. 2000; Ortega et al. 2002; Fullbright 2002; Bensby et al. 2003).

We derived nickel (iron-peak element) and silicium (α-element) abundances for the stars studied in this paper. As in SA08, we selected these two elements because the corresponding spectral lines are not considerably affected by non-LTE effects. The derived abundances are given in Table 5. Additionally, the average abundance [X/H] of all the sample along with the standard deviations and the average number of spectral lines used for each species within each studied association is also given in Table 6.

In Fig. 7, we compare our results with those from GI06 for a sample of stars with and without planetary-mass companions in the solar neighborhood. Because Fe is believed to be a good indicator of the evolutionary state of an association it is extremely useful to plot [X/Fe] against [Fe/H] because it defines a plane where we can compare our results with previous studies taking this element as a reference. From Fig. 7, we can see that the abundance ratios of Si and Ni agree reasonably well with the ratios displayed by the comparison samples. For the range of [X/Fe] ratios covered by our sample, there is almost complete overlap between the data points of the two studies.

In contrast to Si, the nickel abundances disagree slightly from the main trend shown by the comparison sample. Our results are marginally lower than those obtained for MS stars by GI06. At this point, we cannot find an explanation for this small discrepancy which might reflect simply small systematic errors in the analysis.

As concluded by SA08 for the nearby SFRs, our results show that no clear differences exist between the abundance ratios of the studied associations and those of field stars of the same metallicity. The chemical abundances for the combined young sample (SFRs from SA08 and the young associations of this paper) seem to reflect those of typical thin-disk stars.

5. Conclusions

We have determined precise abundances for iron, silicium, and nickel for 63 stars belonging to nearby young associations. While the main aim of this study was to search for a high metallicity sample within these associations, we were unable to detect any metal overabundance in the combined sample of young stars (from this paper and those from SA08), where [Fe/H] has been derived.

Because both groups of WTTS and PTTS in the two samples have not experienced significant spatial displacements, our results imply that the high-metallicity stars harboring planets were not formed in the solar neighborhood but were instead carried to their present position by Galactic dynamical forces.

The Ni and Si abundances derived here are compatible with the general trend observed for the thin-disk stellar population.

Acknowledgements. P.V.A. and J.F.G. were financially supported by the FCT project PTDC/CTE-AST/65971/2006. N.C.S. would like to thank the support from Fundação para a Ciência e a Tecnologia, Portugal through programme Ciência 2007 (C2007-CAUP-FCT/136/2006). M.A.v.E. is supported by an individual fellowship (reference SFRH/BPD/26817/2006) granted by the Fundação para a Ciência e a Tecnologia (FCT), Portugal. M.A.v.E. would like to thank Klaus Fuhrmann who supplied software and model atmospheres for the analysis of the Balmer lines. Furthermore Andreas Korn is thanked for providing a program for the co-addition of spectra.

References

Anders, E., & Grevesse, N. 1989, Geochim, Cosmochim. Acta, 53, 197
Ammler, M. 2006, Ph.D. Thesis, University of Jena
Ammler-von Eiff, M., & Santos, N. C. 2008, AN, 329, 573
Barrado y Navascués, D. 1998, Ap&SS, 263, 235
Bensby, T., Feltzing, S., & Lundström, I. 2003, A&A, 410, 527
Clayton, D. D., & Nittler, L. R. 2004, in Origin and Evolution of the Elements, ed. A. McWilliam, & M. Rauch (Cambridge University Press), 297
Dekker, H., D'Odorico, S., Kaufer, A., Delabre, B., & Kotzlowski, H. 2000, SPIE, 4008, 534
ESA 1997, The Hipparcos and Tycho Catalogues, ESA SP-1200
Feigelson, E. D., & Montmerle, T. 1999, ARA&A, 37, 363
Fischer, D., & Valenti, J. 2005, ApJ, 622, 1102
Flower, P. J. 1996, ApJ, 469, 355
Fuhrmann, K. 2004, Astron. Nachr., 325, 3
Fulbright, J. P. 2002, AJ, 123, 404
Gilli, G., Israelian, G., Ecuvillon, A., Santos, N. C., & Mayor, M. 2006, ApR, 449, 723
Gonzalez, G. 1997, MNRAS, 285, 403
Gonzalez, G. 1998, A&A, 334, 221
Gonzalez, G., Laws, C., Tyagi, S., & Reddy, B. E. 2001, AJ, 121, 432
Gregorio-Hetem, J., Lepine, J. R. D., Quast, G. R., Torres, C. A. O., & de La Reza, R. 1992, AJ, 103, 549
Herbig, G. H. 1978, in Problems of Physics and Evolution of the Universe, ed. L. V. Mirzoyan (Erevan: Armenian Acad. Sci.), 171
James, D. J., Melo, C., Santos, N. C., & Bouvier, J. 2006, A&A, 446, 971
Kasting, J. F., & Catling, D. 2003, ARA&A, 41, 429
Kastner, J. H., Zuckerman, B., Weintraub, D. A., & Forveille, T. 1997, Science, 277, 67
Kurucz, R. 1993, ATLAS9 Stellar Atmosphere Programs and 2 km/s grid, Kurucz CD-ROM No. 13, Cambridge, Mass.: Smithsonian Astrophysical Observatory, 13
Mamajek, E. E., Lawson, W. A., & Feigelson, E. D. 1999, ApJ, 516, 77
Mamajek, E. E., Lawson, W. A., & Feigelson, E. D. 2000, ApJ, 544, 356

McWilliam, A. 1997, ARA&A, 35, 503
Morel, T., Micela, G. F., & Katz, D. 2004, A&A, 426, 1007
Neuhäuser, R., Walter, F. M., Covino, E., et al. 2000, A&AS, 146, 323
Nissen, P. E., Chen, Y. Q., Shuster, W. J., & Zhao, G. 2000, A&A, 353, 722
Ortega, V. G., de la Reza, R., Jilinski, & E., Bazzanella 2002, ApJ, 575, L75
Padgett, D. L. 1996, ApJ, 471, 847
Pollack, J. B., Hubickyj, O., Bodenheimer, P., et al. 1996, Icarus, 124, 62
Santos, N. C., Israelian, G., & Mayor, M. 2001, A&A, 373, 1019
Santos, N. C., Israelian, G., & Mayor, M. 2004, A&A, 415, 1153
Santos, N. C., Israelian, G., Mayor, M., et al. 2005, A&A, 437, 1127
Santos, N. C., Ecuvillon, A., Israelian, G., et al. 2006, A&A, 458, 997
Santos, N. C., Melo, C., James, D. J., et al. 2008, A&A, 480, 889
Schaerer, D., Meynet, G., Maeder, A., et al. 1992, A&AS, 98, 523
Schaerer, D., Charbonnel, C., Meynet, G., et al. 1993, A&AS, 102, 339
Schaller, G., Schaerer, D., Meynet, G., & Maeder, A. 1992, A&AS, 96, 269
Sneden, C. 1973, Ph.D. Thesis, Univ. of Texas
Song, I., Zuckermann, B., & Bessel, M. S. 2003, ApJ, 599, 342
Sousa, S. G., Santos, N. C., Mayor, M., et al. 2008, A&A, 487, 373
Spangler, C., Sargent, A. I., Silverstone, M. D., Becklin, E. E., & Zuckerman, B. 2001, ApJ, 555, 932
Torres, C. A. O., Quast, G. R., de La Reza, R., & Jilinsky, E. 2000, AJ, 120, 1410
Torres, C. A. O., Quast, G. R., de La Reza, R., et al. 2003, in Open Issues in Local Star Formation, ed. J. Lépine, & J. Gregorio-Hetem (Kluwer Academic Publishers), 299, 83
Torres, C. A. O., Quast, G. R., da Silva, L., et al. 2006, AAP, 460, 695
Torres, C. A. O., Quast, G. R., Melo, C. H. F., & Sterzik, M. 2008, [arXiv:0808.3362]
Wielen, R., Fuchs, B., & Dettbarn, C. 1996, A&A, 314, 438
Zuckerman, B., & Song, I. 2004, ARA&A, 42, 685
Zuckermann, B., & Webb, R. A. 2000, ApJ, 535, 959
Zuckermann, B., Song, I., Bessel, M. S., & Webb, R. A. 2001, ApJ, 562, L87
Zuckerman, B., Song, I., & Bessell, M. S. 2004, ApJ, 613, L65

Table 1. Stellar objects used in this study, their coordinates, V magnitude, and the projected rotational velocity $\upsilon \sin i$. High probability members proposed for the different associations are identified with an H in the last column. The remaining stars are possible members (P).

Star	RA (α_{2000})	Dec (δ_{2000})	V (mag)	$\upsilon \sin i$ [km s^{-1}]	P
	AB Dor	Association			
CD-12 243	01 20 32.3	–11 28 04	8.43	3	H
CD-40 1701	05 02 30.4	–39 59 13	10.57	6	H
HD 37572	05 36 56.9	–47 57 53	7.84	9	H
HD 37551A	05 37 12.9	–42 42 56	9.55	5	H
HD 37551B	05 37 13.2	–42 42 57	10.65	5	H
CD-34 2676	06 08 33.9	–34 02 55	10.17	13	H
CD-84 80	07 30 59.5	–84 19 28	9.96	4	H
HD 64982	07 45 35.6	–79 40 08	8.96	14	H
TYC 8243 2975 1	12 30 29.6	–52 22 27	12.04	5	P
HD 207278	21 48 48.5	–39 29 09	9.66	9	H
HD 217343	23 00 19.3	–26 09 14	7.49	12	H
HD 218860A	23 11 52.1	–45 08 11	8.75	6	H
	Argus	Association			
CD-29 2360	05 34 59.2	–29 54 04	10.64	11	P
CD-28 3434	06 49 45.4	–28 59 17	10.38	6	H
CD-42 2906	07 01 53.4	–42 27 56	10.61	10	H
TYC 8561 0970 1	07 53 55.5	–57 10 07	11.50	5	H
BD-20 2977	09 39 51.4	–21 34 17	10.22	10	H
CD-39 5833	09 47 19.9	–40 03 10	10.89	10	H
CD-52 10232	22 39 30.3	–52 05 17	10.85	8	H
	β Pic	Association			
HD 322990	17 16 07.7	-37 28 27	11.46	10	P
	Carina	Association			
TYC 8862 0019 1	02 58 04.0	–62 41 14	11.67	7	P
HD 44627	06 19 12.9	–58 03 16	9.13	11	H
TYC 9178 0284 1	06 55 25.2	–68 06 21	11.91	11	P
HD 55279	07 00 30.5	–79 41 46	10.11	9	H
CD-57 1709	07 21 23.7	–57 20 37	10.72	11	H
CD-55 2543	09 09 29.4	–55 38 27	10.20	13	H
HD 298936	10 13 14.8	–52 30 54	9.79	9	P
	Columba	Association			
HD 26980	04 14 22.6	–38 19 02	9.08	13	H
HD 27679	04 21 10.3	–24 32 21	9.43	11	H
CD-36 1785	04 34 50.8	–35 47 21	10.84	8	H
HD 32372	05 00 51.9	–41 01 07	9.50	7	H
HD 274561	05 28 55.1	–45 34 58	11.45	7	H
CD-40 2458	06 26 06.9	–41 02 54	10.00	12	H
	R CrA	Association			
CD-37 12759	18 39 05.3*	–37 26 22	10.98	9	H
CD-36 13163	18 57 20.8*	–36 43 01	11.04	10	H
	ϵ Cha	Association			
HD 105923	12 11 38.1	–71 10 36	9.16	12	H
	LCC	Association			
CP-52 5025	11 55 57.7	–52 54 01	11.00	6	H
CD-49 4947	12 12 11.2	–49 50 08	11.37	14	H
CP-64 1859	12 19 21.6	–64 54 10	9.87	13	P
CD-51 6900	12 40 46.6	–52 11 05	11.91	14	H
CD-40 7581	12 56 12.3	–41 22 20	11.73	13	H
CD-40 8031	13 37 57.3	–41 34 42	10.12	13	H
CP-66 2366	13 54 07.4	–67 33 45	10.93	11	P
	Octans	Association			
HD 23208	03 42 39.8	–20 32 44	9.16	10	P

Table 1. continued.

Star	RA (α_{2000})	Dec (δ_{2000})	V (mag)	$\upsilon \sin i$ [km s^{-1}]	P
	Tuc-Hor Association				
HD 105	00 05 52.5	–41 45 11	7.53	12	H
HD 987	00 13 53.0	–74 41 18	8.78	7	H
HD 8558	01 23 21.3	–57 28 51	8.51	14	H
HD 9054	01 28 08.7	–52 38 19	9.07	4	H
CD-46 1064	03 30 49.1	–45 55 57	9.55	10	H
HD 47875	06 34 41.0	–69 53 06	9.17	11	P
CD-38 4458	08 26 10.0	–39 02 05	10.31	9	P
HD 202917	21 20 50.0	–53 02 03	8.69	14	H
HD 222259B	23 39 39.3	–69 11 40	9.84	14	H
	US Association				
CD-34 10180	15 07 14.8	–35 05 00	10.53	13	H
CD-36 10208	15 29 47.3	–36 28 37	11.16	14	H
TYC 9034 0968 1	15 33 27.5	–66 51 25	10.99	5	H
CD-39 10162	15 47 41.8	–40 18 27	11.08	12	H
CD-25 11330	16 05 50.6	–25 33 14	10.93	8	H
CD-22 11502	16 19 34.0	–22 28 29	11.11	12	H
CD-51 10295	16 33 50.4	–51 19 01	10.75	4	H
CD-31 13486	17 02 27.8	–32 04 36	10.13	13	H
CD-23 13281	17 16 18.1	–23 10 47	10.97	14	H
TYC7886 1894 1	17 58 31.5	–37 43 03	11.62	5	H

Table 2. The determined atmospheric parameters $T_{\rm eff}$, log g, [Fe/H], $\xi_{\rm t}$ for each star. In the last three columns, we show the number of Fe lines used in each determination, the average uncertainty in the abundances given by each line EW.

Star	$T_{\rm eff}$ [K]	log g [cm s^{-2}]	$\xi_{\rm t}$ [km s^{-1}]	[Fe/H]	[Fe/H]*	N (FeI , FeII)	σ (FeI , FeII)
			AB Dor Association				
CD-12 243	5406 ± 38	4.67 ± 0.09	1.21 ± 0.02	0.00 ± 0.05	0.04	37 , 10	0.05 , 0.03
CD-40 1701	4800 ± 80	4.61 ± 0.24	1.68 ± 0.14	−0.11 ± 0.08	0.01	36 , 8	0.08 , 0.10
HD 37572	5251 ± 43	4.45 ± 0.11	1.82 ± 0.07	−0.11 ± 0.06	−0.05	34 , 6	0.05 , 0.05
HD 37551A	5684 ± 32	4.52 ± 0.07	1.46 ± 0.05	0.05 ± 0.04	0.06	33 , 12	0.04 , 0.03
HD 37551B	5055 ± 68	4.31 ± 0.14	1.65 ± 0.08	−0.03 ± 0.08	0.06	36 , 8	0.07 , 0.06
CD-34 2676	5571 ± 86	4.47 ± 0.20	2.08 ± 0.14	−0.01 ± 0.10	0.01	32 , 8	0.08 , 0.08
CD-84 80	5381 ± 45	4.53 ± 0.16	1.53 ± 0.07	−0.05 ± 0.05	0.00	38 , 12	0.05 , 0.07
HD 64982	6106 ± 72	4.14 ± 0.30	1.53 ± 0.13	0.10 ± 0.09	0.05	32 , 12	0.07 , 0.12
TYC 8243 2975 1	4626 ± 74	4.16 ± 0.22	1.35 ± 0.11	−0.19 ± 0.07	−0.04	31 , 6	0.07 , 0.09
HD 207278	5714 ± 52	4.51 ± 0.10	1.45 ± 0.08	0.08 ± 0.06	0.08	33 , 9	0.05 , 0.05
HD 217343	5795 ± 41	4.44 ± 0.09	1.68 ± 0.08	0.00 ± 0.05	−0.01	34 , 10	0.04 , 0.05
HD 218860A	5550 ± 68	4.50 ± 0.13	1.42 ± 0.05	0.10 ± 0.06	0.13	34 , 12	0.05 , 0.05
			Argus Association				
CD-29 2360	4917 ± 77	4.66 ± 0.16	1.92 ± 0.12	0.04 ± 0.07	0.15	32 , 5	0.08 , 0.06
CD-28 3434	5652 ± 39	4.51 ± 0.13	1.62 ± 0.07	−0.01 ± 0.05	0.00	35 , 11	0.04 , 0.06
CD-42 2906	5308 ± 49	4.38 ± 0.13	1.76 ± 0.07	−0.03 ± 0.07	0.03	36 , 8	0.06 , 0.06
TYC 8561 0970 1	5348 ± 51	4.48 ± 0.15	1.75 ± 0.07	−0.07 ± 0.07	−0.02	38 , 12	0.06 , 0.06
BD-20 2977	5421 ± 50	4.50 ± 0.14	2.05 ± 0.09	−0.09 ± 0.06	−0.05	33 , 10	0.05 , 0.07
CD-39 5833	5471 ± 61	4.45 ± 0.12	1.72 ± 0.10	0.01 ± 0.07	0.05	35 , 9	0.07 , 0.05
CD-52 10232	5381 ± 59	4.48 ± 0.13	1.83 ± 0.09	−0.06 ± 0.07	−0.01	35 , 10	0.07 , 0.06
			β Pic Association				
HD 322990	4858 ± 74	4.20 ± 0.20	2.05 ± 0.10	−0.13 ± 0.08	−0.01	31 , 9	0.08 , 0.10
			Carina Association				
TYC 8862 0019 1	4776 ± 120	4.38 ± 0.47	2.29 ± 0.2	−0.14 ± 0.14	−0.01	38 , 10	0.14 , 0.25
HD 44627	5156 ± 54	4.29 ± 0.17	1.90 ± 0.06	−0.01 ± 0.06	0.07	30 , 8	0.05 , 0.08
TYC 9178 0284 1	4607 ± 89	3.98 ± 0.36	1.90 ± 0.12	−0.10 ± 0.08	0.05	28 , 6	0.08 , 0.19
HD 55279	4918 ± 50	4.19 ± 0.18	1.85 ± 0.07	−0.08 ± 0.05	0.03	33 , 8	0.05 , 0.08
CD-57 1709	5368 ± 55	4.58 ± 0.19	1.85 ± 0.08	−0.06 ± 0.06	−0.01	33 , 10	0.05 , 0.09
CD-55 2543	5512 ± 53	4.38 ± 0.20	1.70 ± 0.08	−0.05 ± 0.06	−0.02	31 , 8	0.05 , 0.09
HD 298936	4923 ± 119	4.47 ± 0.29	1.96 ± 0.14	−0.08 ± 0.08	0.03	30 , 8	0.06 , 0.08
			Columba Association				
HD 26980	5910 ± 61	4.26 ± 0.12	1.74 ± 0.12	−0.01 ± 0.07	−0.03	34 , 10	0.07 , 0.06
HD 27679	5817 ± 58	4.16 ± 0.31	1.96 ± 0.13	−0.04 ± 0.08	−0.05	37 , 12	0.07 , 0.14
CD-36 1785	5276 ± 48	4.31 ± 0.19	2.63 ± 0.09	−0.15 ± 0.06	−0.09	32 , 7	0.05 , 0.09
HD 32372	5716 ± 50	4.31 ± 0.09	1.89 ± 0.10	−0.07 ± 0.07	−0.07	38 , 11	0.06 , 0.04
HD 274561	5144 ± 63	4.36 ± 0.12	2.09 ± 0.10	−0.11 ± 0.07	−0.03	30 , 7	0.06 , 0.05
CD-40 2458	5415 ± 62	4.32 ± 0.19	1.98 ± 0.09	0.06 ± 0.08	0.1	34 , 9	0.07 , 0.09
			R CrA Association				
CD-37 12759	5149 ± 104	4.28 ± 0.30	1.98 ± 0.15	−0.08 ± 0.13	0.00	35 , 10	0.07 , 0.07
CD-36 13163	5098 ± 44	3.99 ± 0.13	1.73 ± 0.05	−0.08 ± 0.06	0.00	31 , 9	0.05,0.07
			ϵ Cha Association				
HD 105923	4979 ± 40	3.98 ± 0.13	1.94 ± 0.06	0.01 ± 0.05	0.03	32 , 8	0.05 , 0.06
			LCC Association				
CP-52 5025	4834 ± 78	4.19 ± 0.18	1.69 ± 0.10	−0.07 ± 0.07	0.05	28 , 7	0.07 , 0.06
CD-49 4947	4875 ± 56	4.17 ± 0.20	2.21 ± 0.07	−0.08 ± 0.06	0.03	28 , 6	0.06 , 0.10
CP-64 1859	5422 ± 145	5.14 ± 0.25	1.46 ± 0.25	−0.08 ± 0.13	0.03	30 , 7	0.11 , 0.09
CD-51 6900	4842 ± 71	3.98 ± 0.18	2.04 ± 0.10	−0.15 ± 0.08	−0.03	29 , 4	0.07 , 0.08
CD-40 7581	4979 ± 69	4.20 ± 0.13	1.80 ± 0.08	0.01 ± 0.07	0.11	30 , 4	0.07 , 0.04
CD-40 8031	5243 ± 55	4.06 ± 0.21	1.78 ± 0.07	−0.03 ± 0.07	0.04	31 , 7	0.06 , 0.10
CP-66 2366	5793 ± 75	4.89 ± 0.34	2.15 ± 0.15	−0.03 ± 0.08	−0.04	25 , 9	0.06 , 0.15
			Octans Association				
HD 23208	5322 ± 43	4.23 ± 0.14	1.85 ± 0.06	−0.09 ± 0.06	−0.03	34 , 8	0.05 , 0.07
			Tuc-Hor Association				
HD 105	6012 ± 68	4.42 ± 0.12	1.24 ± 0.12	0.06 ± 0.09	0.02	36 , 8	0.07 , 0.05

Table 2. continued.

Star	$T_{\rm eff}$ [K]	log g [cm s^{-2}]	$\xi_{\rm t}$ [km s^{-1}]	[Fe/H]	[Fe/H]*	N (FeI , FeII)	σ (FeI , FeII)
HD 987	5488 ± 46	4.36 ± 0.12	1.85 ± 0.08	−0.07 ± 0.06	−0.04	35 , 11	0.05 , 0.06
HD 8558	5538 ± 53	4.04 ± 0.16	1.90 ± 0.09	−0.09 ± 0.07	−0.06	30 , 7	0.06 , 0.07
HD 9054	5045 ± 55	4.49 ± 0.15	1.90 ± 0.07	−0.08 ± 0.06	0.01	31 , 9	0.05 , 0.07
CD-46 1064	4777 ± 70	4.13 ± 0.18	1.92 ± 0.10	−0.16 ± 0.07	−0.03	33 , 6	0.07 , 0.07
HD 47875	5781 ± 35	4.53 ± 0.17	1.75 ± 0.07	0.01 ± 0.05	0.00	33 , 9	0.04 , 0.07
CD-38 4458	5751 ± 34	4.32 ± 0.11	1.60 ± 0.06	0.03 ± 0.05	0.03	35 , 10	0.04 , 0.05
HD 202917	5592 ± 79	4.31 ± 0.17	2.16 ± 0.15	−0.06 ± 0.10	−0.04	33 , 9	0.08 , 0.07
HD 222259B	4938 ± 91	4.12 ± 0.26	2.59 ± 0.15	−0.22 ± 0.09	−0.11	27 , 8	0.08 , 0.12
			US Association				
CD-34 10180	5188 ± 49	4.05 ± 0.20	2.30 ± 0.08	−0.11 ± 0.07	−0.04	34 , 8	0.06 , 0.10
CD-36 10208	4869 ± 71	3.64 ± 0.23	2.59 ± 0.10	−0.27 ± 0.07	−0.16	27 , 5	0.07 , 0.11
TYC 9034 0968 1	4955 ± 65	4.52 ± 0.47	1.80 ± 0.07	−0.11 ± 0.11	−0.01	33 , 9	0.07 , 0.13
CD-39 10162	4922 ± 61	4.05 ± 0.14	2.04 ± 0.09	−0.14 ± 0.08	−0.03	33 , 7	0.07 , 0.10
CD-25 11330	5076 ± 62	4.14 ± 0.18	2.02 ± 0.09	−0.16 ± 0.07	−0.07	34 , 11	0.06 , 0.08
CD-22 11502	4951 ± 66	3.81 ± 0.17	2.10 ± 0.08	−0.18 ± 0.07	−0.08	34 , 9	0.07 , 0.08
CD-51 10295	4922 ± 58	4.31 ± 0.20	1.59 ± 0.07	−0.08 ± 0.05	0.03	31 , 6	0.06 , 0.10
CD-31 13486	5625 ± 42	4.55 ± 0.25	1.68 ± 0.07	0.01 ± 0.06	0.03	35 , 10	0.06 , 0.11
CD-23 13281	4900 ± 84	4.41 ± 0.26	2.14 ± 0.32	0.08 ± 0.17	0.19	28 , 6	0.08 , 0.10
TYC 7886 1894 1	5048 ± 62	4.26 ± 0.18	2.16 ± 0.09	−0.18 ± 0.07	−0.09	33 , 9	0.06 , 0.08

Table 5. Derived abundances of Si and Ni for the stars in the sample.

Star	[Si/H]	σ	N	[Ni/H]	σ	N
		AB Dor				
CD-12 243	−0.05	0.03	9	−0.05	0.04	25
CD-40 1701	−0.08	0.10	7	−0.16	0.10	24
HD 37572	−0.09	0.04	9	−0.02	0.07	25
HD 37551A	0.04	0.04	9	0.02	0.06	30
HD 37551B	−0.02	0.04	9	0.02	0.07	27
CD-34 2676	−0.14	0.09	9	−0.06	0.09	20
CD-84 80	−0.05	0.04	9	−0.04	0.05	25
HD 64982	0.02	0.07	9	−0.26	0.14	22
TYC 8243 2975 1	−0.23	0.08	6	−0.10	0.18	24
HD 207278	0.05	0.03	9	0.13	0.08	27
HD 217343	−0.05	0.05	9	0.07	0.06	22
HD 218860A	0.06	0.03	9	0.1	0.07	29
		Argus				
CD-29 2360	−0.02	0.09	9	−0.03	0.08	20
CD-28 3434	−0.04	0.04	9	−0.01	0.06	28
CD-42 2906	−0.07	0.07	9	0.06	0.06	26
TYC 8561 0970 1	−0.09	0.04	9	−0.01	0.06	27
BD-20 2977	−0.1	0.06	9	−0.01	0.07	22
CD-52 10232	−0.05	0.03	9	0.04	0.08	26
CD-39 5833	−0.07	0.05	9	0.08	0.07	27
		β Pic				
HD 322990	−0.1	0.13	9	0.02	0.09	23
		Carina				
TYC 8862 0019 1	−0.11	0.13	8	−0.10	0.12	21
HD 44627	−0.02	0.10	9	0.10	0.09	24
TYC 9178 0284 1	−0.07	0.12	8	0.05	0.11	19
HD 55279	−0.07	0.07	9	−0.01	0.08	23
CD-57 1709	−0.09	0.07	8	0.01	0.08	24
CD-55 2543	−0.13	0.07	8	0.00	0.11	18
HD 298936	−0.08	0.11	9	−0.05	0.09	22
		Columba				
HD 26980	−0.1	0.08	8	−0.16	0.06	17
HD 27679	−0.09	0.06	8	0.11	0.10	21
CD-36 1785	−0.18	0.08	9	0.06	0.08	25
HD 32372	−0.12	0.04	9	0.06	0.06	27
HD 274561	−0.15	0.07	9	0.04	0.08	25
CD-40 2458	−0.08	0.08	7	0.15	0.09	24
		R CrA				
CD-37 12759	−0.09	0.08	9	0.04	0.08	22
CD-36 13163	−0.06	0.06	9	0.05	0.09	25
		ϵ Cha				
HD 105923	–	–	–	–	–	–
		LCC				
CP-52 5025	−0.14	0.10	8	0.10	0.09	23
CD-49 4947	−0.15	0.10	5	−0.08	0.13	15
CP-64 1859	−0.24	0.18	7	−0.13	0.13	17
CD-51 6900	−0.19	0.08	8	0.03	0.11	19
CD-40 7581	−0.09	0.11	9	0.07	0.12	24
CD-40 8031	−0.1	0.09	8	0.07	0.09	18
CP-66 2366	−0.10	0.07	7	−0.04	0.06	15
		Octans				
HD 23208	−0.08	0.09	9	0.02	0.08	27
		Tuc-Hor				
HD 105	−0.06	0.07	9	0.16	0.17	20
HD 987	−0.12	0.04	9	0.06	0.09	28

Table 5. continued.

Star	[Si/H]	σ	N	[Ni/H]	σ	N
HD 8558	−0.46	0.31	3	−0.4	0.34	11
HD 9054	−0.09	0.08	9	−0.06	0.08	23
CD-46 1064	−0.11	0.11	9	−0.07	0.10	21
HD 47875	−0.05	0.06	9	0.14	0.11	22
CD-38 4458	−0.02	0.09	9	0.12	0.07	26
HD 202917	−0.17	0.06	8	0.05	0.17	23
HD 222259B	−0.49	0.14	6	0.00	0.17	19
		US				
CD-34 10180	−0.19	0.09	8	0.1	0.12	22
CD-36 10208	−0.41	0.11	6	0.07	0.13	20
TYC 9034 0968 1	−0.14	0.11	9	−0.1	0.10	25
CD-39 10162	−0.14	0.09	9	−0.03	0.10	24
CD-25 11330	−0.18	0.06	9	−0.02	0.11	27
CD-22 11502	−0.20	0.07	8	0.04	0.11	23
CD-51 10295	−0.09	0.08	9	0.00	0.10	25
CD-31 13486	−0.04	0.04	9	0.07	0.09	25
CD-23 13281	−0.03	0.10	8	0.07	0.16	24
TYC 7886 1894 1	−0.16	0.08	9	0.09	0.16	29